ACS MATERIALS LETTERS

www.acsmaterialsletters.org

Crystal Structure Control of the Energetics of Chemical Doping in Rub-Aligned P3HT Films

Yutong Wu, Quynh M. Duong, Alexander F. Simafranca, Charlene Z. Salamat, Benjamin J. Schwartz,* and Sarah H. Tolbert*

Cite This: *ACS Materials Lett.* 2024, 6, 489–497

Read Online

ACCESS | Metrics & More | Article Recommendations | Supporting Information

ABSTRACT: Semiconducting polymers have received increased attention in recent years as low-cost, electrically conductive layers. To show reasonable electrical conductivity, however, semiconducting polymers must be doped, a process that requires oxidation or reduction of the conjugated backbone and structural rearrangement to accommodate a charge-balancing counterion into the polymer network. Here, we aim to understand how this structural rearrangement contributes to the energetics of doping. We utilize the fact that rub-aligned poly(3-hexylthiophene-2,5-diyl) (P3HT) films contain two polymorphs, one with a crystal structure that is less dense than the structure observed in unaligned films and the other with a more compact, denser structure. The two structures are dominantly face-on and edge-on with respect to the substrate, respectively, so their diffraction is well separated in *q*-space and thus doping induced structural changes can be monitored separately for each population. When films are doped with 2,3,5,6-tetrafluoro-7,7,8,8-tetracyanoquinodimethane (F_4TCNQ), the less-dense face-on oriented P3HT polymorph undergoes doping induced structural change more easily than the denser edge-on oriented polymorph. This finding suggests that rearrangement of the polymer crystal structure to accommodate the dopant counterion is a significant energetic term in the doping process and that doping of semiconducting polymers can be facilitated by designing new polymers where dopant counterions can be accommodated in the polymer lattice with reduced structural change.

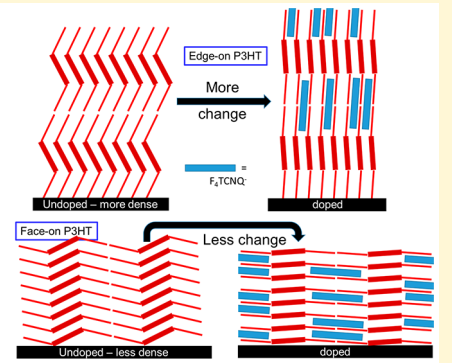

Semiconducting polymers are predicted to find wide use in future electronic devices because of their low cost, versatility, scalability, and solution processability.[1−8] Undoped semiconducting polymers are inherently poor electrical conductors due to their wide band gaps and low density of intrinsic charge carriers.[9] As a result, doping is required to generate carriers and make semiconducting polymers more conductive.[10] Similar to impurity doping in inorganic semiconductors, doping in semiconducting polymers occurs via charge transfer between the polymer and dopant molecules that are introduced into the polymer film.[11] Electrons can be either injected into the polymer conduction band (*n*-type) or withdrawn from the polymer valence band (*p*-type) to determine the majority carrier type.[12,13] Most studies focus on *p*-type semiconducting polymers due to their higher stability in air compared to *n*-type materials.[14]

In addition to selecting a dopant with a redox level that matches or exceeds the valence band energy of a semiconducting polymer, it is also critical to understand the structural changes of the polymer that take place during dopant introduction. Semiconducting polymer films are usually semicrystalline, containing both crystalline and amorphous regions.[15] Our previous work has shown that the polymer's degree of crystallinity can significantly affect charge carrier mobility by controlling where the dopants reside in the polymer film's structure.[16] Compared with amorphous regions, crystalline regions are generally easier to dope, and the resulting carriers have higher mobilities.[16,17] This means that the doped polymer film conductivity is governed by the structure and extent of the crystalline regions.[18]

It has been well established that when semiconducting polymers are doped, dopant molecules almost always intercalate into the lamellar side-chain regions of the polymer crystallites.[16,19−22] Due to limited space in the lamellar region, the crystallite structure often undergoes a phase transition to accommodate the dopant molecules, resulting in a new packing geometry with a wider lamellar region, less tilting of the side

Received: December 7, 2023
Revised: December 14, 2023
Accepted: December 14, 2023

https://doi.org/10.1021/acsmaterialslett.3c01543
ACS Materials Lett. 2024, 6, 489–497

chains with respect to the π-stacks, and an overall less dense packing of polymer chains.[16,20,23] Many doped conjugated polymer systems, including doped polymers that have undergone anion exchange, exhibit such a structural rearrangement.[19,20,24−26] Our previous work showed that even very large (~2 nm diameter) dodecaborane-based dopants intercalate into the lamellar side-chain region of polymer crystallites, in this case leading to a near doubling of the crystallite lamellar spacing.[17,27] Intercalation of dopants into the side chain region does not happen if there is a steric hindrance in this region or if the processing conditions allow planar dopants such as 2,3,5,6-tetrafluoro-7,7,8,8-tetracyanoquinodimethane (F_4TCNQ) to π-stack with the polymer backbone, changing the nature of the doping.[28−30]

Among doped semiconducting polymers, the F_4TCNQ-doped poly(3-hexylthiophene-2,5-diyl) (P3HT) system is one of the most studied. P3HT crystallites have a monoclinic unit cell with side chains that are tipped away from the aromatic ring plane to better fill space.[31] When cast as a thin film, P3HT has been shown to form both edge-on (i.e., alkyl side chains contacting the substrate) and face-on (i.e., backbone rings contacting the substrate) crystallites depending on the processing conditions and substrate interfacial energy.[32−39] Although as-deposited semiconducting polymer films are typically isotropic with regard to the in-plane rotational angle (φ), there are a number of methods for aligning crystallites within the film, which range from strain-based or float-casting methods to the use of textured substrates.[38,40−44] Work by Brinkmann and co-workers produced aligned P3HT films by rub-alignment, resulting in highly crystalline and aligned polymers. These researchers used electron diffraction (ED) to show that the rub-aligned films have both face-on- and edge-on-oriented P3HT polymorphs.[20,24,30−33] In subsequent studies, they also used aligned films to better understand how the P3HT crystal structure changed upon doping. They found that when F_4TCNQ intercalates into the polymer lamellar side chain region, the side-chain angle relative to the thiophene ring (i.e., the side chain "tilt" angle) is reduced, resulting in an altered unit cell structure characterized by an increased lamellar spacing and a decreased π-stack spacing.[20] We note, however, that the use of ED in their work, which can only probe in-plane periodicity, means that the observed structural changes were based on examining the lamellar distance in the face-on-oriented doped P3HT polymorph and the π-stacking distance in the edge-on-oriented polymorph, so structural differences between the edge-on and face-on-oriented populations could not be discerned.

In this work, we build on these previous studies of structural changes during doping by using grazing-incidence wide-angle X-ray scattering (GIWAXS)[45] to fully characterize the structures of both the edge-on and face-on polymorphs in rub-aligned P3HT films. GIWAXS reveals that although the two polymorphs have similar crystal structures, the chain packing is, in fact, somewhat different. The face-on polymorph has a structure that is less dense than that observed in standard, unaligned P3HT films and thus slightly more similar to the doped structure. Conversely, the rub-aligned edge-on domains appear to be compacted by the alignment process so that they have a denser structure that is even more different from the doped geometry than unaligned P3HT. We then show that the structural changes associated with doping are not a gradual evolution but instead occur as an abrupt first-order phase transition. By starting with a very low dopant concentration and increasing the degree of doping in small steps, we can capture a region where both the undoped and F_4TCNQ-doped P3HT polymorphs coexist. We find that the less-dense P3HT polymorph dopes first, followed by the denser polymorph at higher doping concentrations. We argue that this results from the fact that the denser polymorph must change its crystal structure more to make space for the F_4TCNQ^- counterion, making the doping-induced phase transition harder. This finding demonstrates that even minor variations in the initial polymer crystallite structure strongly influence the ease of doping and suggests a new strategy to design polymers that are easier to dope.

To carry out our studies, we utilized the high-temperature rub-alignment method introduced by Brinkmann and co-workers to obtain highly aligned P3HT films.[46] First, P3HT (Rieke metals, Inc., M_n = 50−70 kg/mol, regioregularity 91−94%) was spin-coated onto glass substrates from 1,2-dichlorobenzene (ODCB) to produce films of uniform thickness. The P3HT films were then rub-aligned using a microfiber wheel while being heated in an inert atmosphere (see the Supporting Information (SI), for more details). The degree of film alignment was characterized using polarized absorption spectroscopy, in which polarized incident light was oriented either parallel (∥) or perpendicular (⊥) to the direction of rub alignment.

Figure 1a shows the polarized visible-NIR absorption spectra of unaligned (yellow curve) and rub-aligned (red curve for ∥ and blue curve for ⊥) P3HT films. The polarized absorbance spectra of the aligned film show significant anisotropy, with a dichroic ratio $I_{\parallel}/I_{\perp}$ = ~14 at 610 nm, comparable to previous rub-aligned P3HT work.[47,48] The absorption spectra of the rub-aligned film in both polarizations are quite different from those of the unaligned film, showing that rub-alignment significantly alters the structure of the film. The absorption spectrum of unaligned P3HT shows a progression of vibronic peaks at 2.03 eV (0−0 transition, A_{0-0}) and 2.23 eV (0−1 transition, A_{0-1}), with an A_{0-0}/A_{0-1} peak ratio of 0.53. The aligned P3HT film shows a parallel-polarized absorption spectrum with a larger A_{0-0}/A_{0-1} peak ratio (0.63). This results from improved intrachain coupling caused by backbone straightening during rub-aligning.[49−51] In the perpendicular-polarized absorption spectrum, rub-aligned P3HT has a blue-shifted absorbance peak with no vibronic features, corresponding to the absorbance of short or amorphous polymer chains that were not successfully oriented by the rub-aligning process.[20]

Although polarized absorption spectroscopy can determine the degree of polymer film alignment, direct structural measurements such as GIWAXS are necessary to provide details on the structure and orientation of the polymer crystallites within the film.[45,52] The crystallites in unaligned P3HT films usually adopt an edge-on orientation with the out-of-plane diffraction peaks corresponding to the lamellar direction and the in-plane diffraction peak corresponding to the π-stacking distance (see Figure S1a).[22] We note that the P3HT monomer repeat distance and double the π-stacking distance have comparable length scales, so these two peaks can sometimes be difficult to distinguish.[20] Figure 2a shows the 2-D GIWAXS diffraction pattern for a rub-aligned P3HT film in which the incident X-ray beam is parallel to the rub-alignment direction. Unlike data collected on unaligned films, both lamellar and π-stacking diffraction peaks are seen in both the in-plane and out-of-plane directions, indicating the coexistence

https://doi.org/10.1021/acsmaterialslett.3c01543
ACS Materials Lett. 2024, 6, 489−497

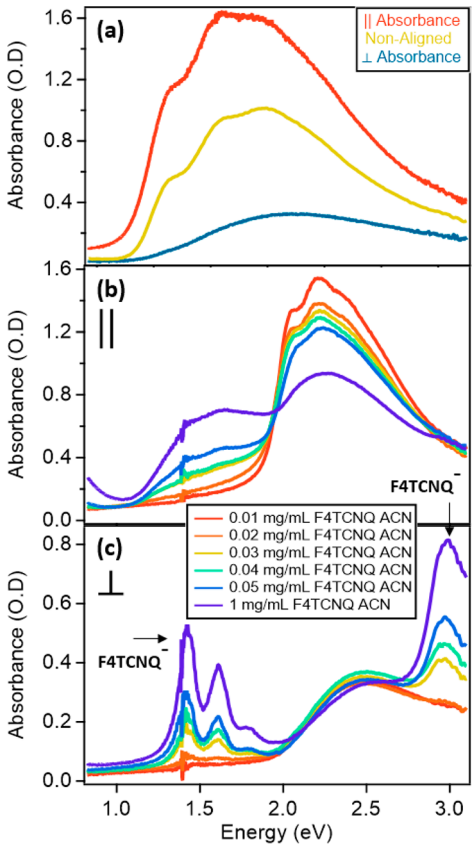

Figure 1. Polarized visible-NIR absorbance of (a) an unaligned P3HT film (yellow curve) and a rub-aligned P3HT film with light polarized parallel (||, red curve) and perpendicular (⊥, blue curve) to the rub direction. The absorption anisotropy of the rub-aligned P3HT film is ∼14 near the absorption maximum, indicating a high degree of chain alignment. Visible-NIR absorption of aligned P3HT sequentially doped with F_4TCNQ at different concentrations using light polarized (b) parallel and (c) perpendicular to the rub-alignment direction. The P2 band observed near 1.5 eV and the decrease of the ∼2.2 eV neutral P3HT absorption seen in the parallel polarization are both indicative of doping and, thus, polaron formation. As seen previously, the polaron absorption is only visible with parallel polarization, while the F_4CTNQ^- absorption only appears with perpendicular polarization, indicating that the long axis of the F_4TCNQ^- molecule is oriented perpendicular to the P3HT backbone, consistent with the conclusions in refs 21 and 45.[20,22]

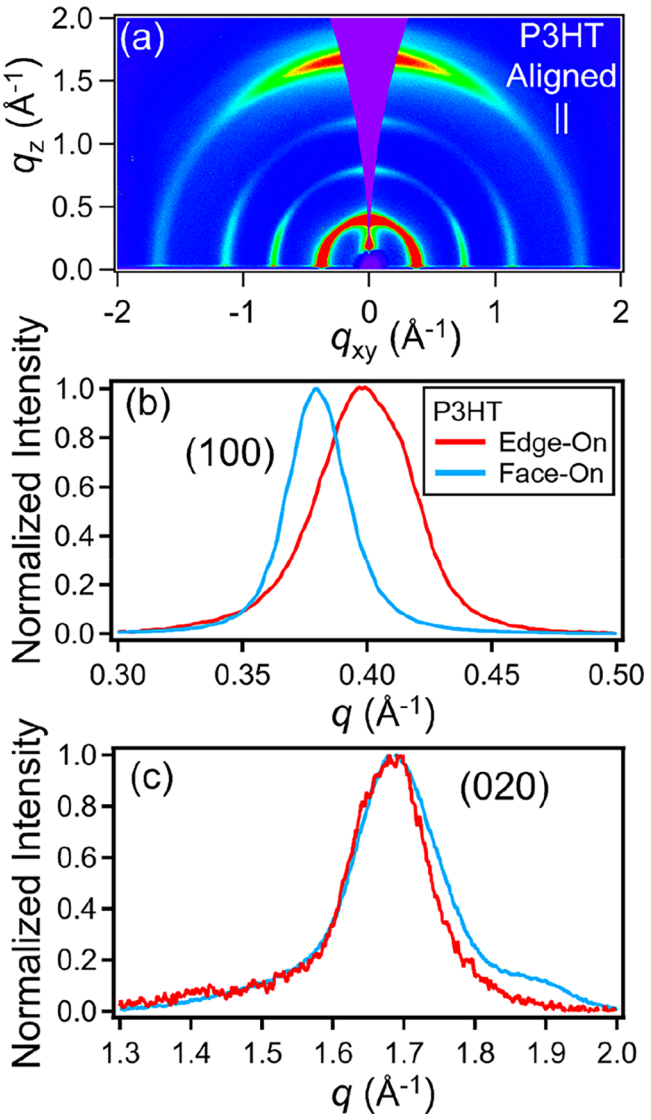

Figure 2. (a) 2-D GIWAXS pattern for rub-aligned P3HT with the beam oriented along the rub direction, showing that unlike unaligned films that have only edge-on-oriented crystallites, the rub-aligned film has both face-on- and edge-on-oriented crystallites. Integrated (b) (100) lamellar and (c) (020) π-stacking peaks of rub-aligned P3HT can be obtained by selective integration of the data in (a) for both the edge-on-oriented (red curves) and face-on-oriented (blue curves) crystallites. The data make clear that the face-on-oriented P3HT crystallites have a larger lamellar side-chain spacing and a slightly smaller π-stacking distance compared to those of the edge-on-oriented crystallites.

of edge-on-oriented and face-on-oriented P3HT polymorphs.[20,48] Radial integration of the diffraction peaks in the in-plane and out-of-plane directions, however, reveals differences between the crystal structures of the face-on-oriented and edge-on-oriented polymorphs. The face-on P3HT polymorph has a larger lamellar distance ($d_{lamellar}$ = 16.64 Å) compared to the edge-on polymorph ($d_{lamellar}$ = 16.03 Å), as seen in Figure 2b,c. In comparison to unaligned P3HT ($d_{lamellar}$ = 16.36 Å), we find that the layer spacing of the face-on polymorph is expanded in a less dense structure, while the layer spacing in the edge-on polymorph is compressed, corresponding to a denser structure (see SI Table S1).

Here, we take advantage of the fact that we can directly observe both the lamellar and π-stacking peaks of the two differently oriented polymorphs to show that these subtle differences in structure between the edge-on and face-on P3HT polymorphs affect the energetics of doping. To examine changes in the crystal structure during doping, we treated rub-aligned P3HT films with very low concentrations of F_4TCNQ and slowly increased the dopant concentrations to capture the doping phase transitions of both the edge-on and face-on P3HT polymorphs.

All films were doped by sequential processing (SqP), in which a precast rub-aligned P3HT film is exposed to the F_4TCNQ using a solvent that swells but does not dissolve the polymer and is then spun off after a brief soaking period. We have shown previously that the SqP doping method largely preserves the initial film morphology in terms of crystallite orientation and film crystallinity.[53] In agreement with this idea, the polarized absorption spectra of rub-aligned P3HT films

https://doi.org/10.1021/acsmaterialslett.3c01543
ACS Materials Lett. 2024, 6, 489−497

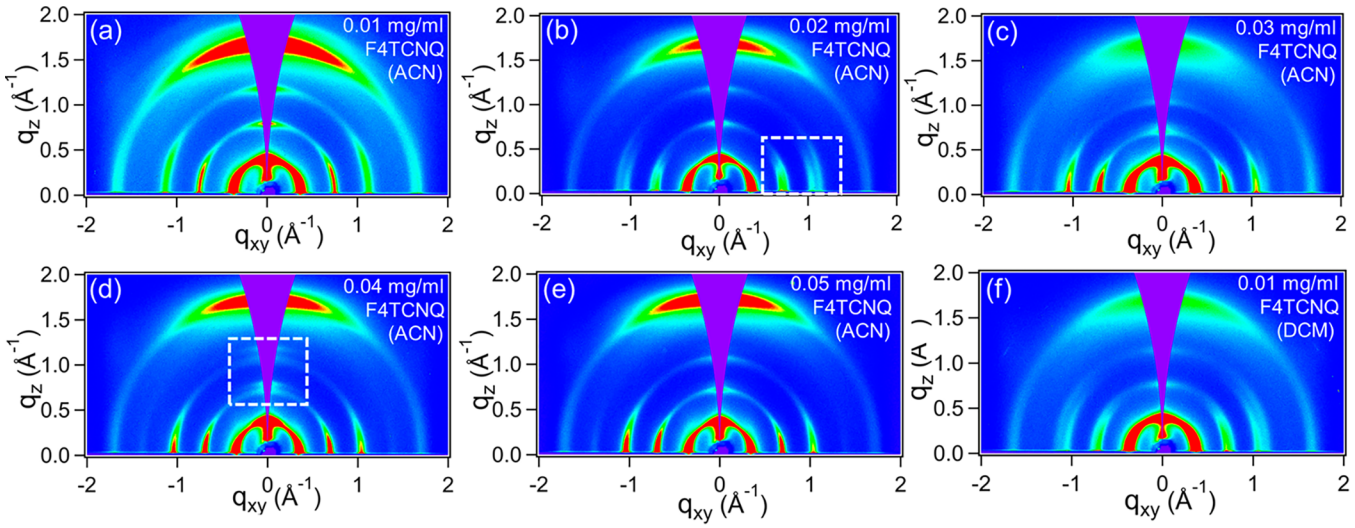

Figure 3. (a)-(e) 2-D GIWAXS patterns of rub-aligned P3HT films sequentially doped with different concentrations of F_4TCNQ in CH_3CN (acetonitrile, ACN), taken with the beam oriented parallel to the rub direction. Face-on-oriented P3HT crystallites dope first, at 0.02 mg/mL F_4TCNQ, followed by the denser edge-on-oriented P3HT crystallites, which dope at 0.04 mg/mL F_4TCNQ. (f) 2-D GIWAXS pattern of rub-aligned P3HT doped with 0.01 mg/mL F_4TCNQ in dichloromethane (DCM). DCM swells the polymer more than does ACN, allowing for faster doping kinetics. In agreement with this idea, the less dense face-on polymorph is already about half doped at this low F_4TCNQ concentration, but the denser edge-on polymorph remains undoped, indicating that the different phase transition points of the two polymorphs are not a kinetic effect. See Figure S3 for the full DCM data set; all of the trends are the same, but values are shifted to lower F_4TCNQ concentrations.

doped with different concentrations of F_4TCNQ are shown in Figure 1b,c; retention of the anisotropic features in each polarization direction confirms that the film alignment is retained through the SqP doping process.[20] As is well documented, doping P3HT bleaches the bandgap transition (~2.25 eV) and generates new intraband electronic states, creating the transition labeled "P2" near 1.6 eV that is seen in the parallel-polarized absorption spectrum shown in Figure 1b.[54] In contrast, the absorption of the F_4TCNQ^- anion is seen predominantly in the perpendicularly polarized absorption spectrum (Figure 1c).[20,22] This difference between parallel- and perpendicular-polarized spectra indicates that the F_4TCNQ dopant counterions sit in the crystallites with their long axis oriented perpendicular to the P3HT backbone.[20,55,56] Taken together, the data in Figure 1 indicate that at these low doping concentrations, the F_4TCNQ dopant is predominantly found within the crystalline regions of the film. This agrees with previous work that also found that crystalline regions of P3HT dope more easily than amorphous regions.[16,57]

We can gain structural insight into the nature of the doping process in these aligned films by using GIWAXS. Figure 3a-e shows GIWAXS diffraction patterns of the doped samples whose spectroscopy is characterized in Figure 1b,c. As seen with the undoped aligned P3HT films, the doped samples exhibit lamellar and π-stacking diffraction peaks in both the in-plane and out-of-plane directions, indicating that the coexistence of face-on- and edge-on-oriented crystallites is retained after sequential doping. When P3HT is initially doped by F_4TCNQ, the undoped P3HT lamellar (h00) peaks shift to a new position at lower q, a process that is the hallmark of a doping-induced phase transition.[16] Structurally, this change corresponds to reduction of the "tilt" of the side chains with respect to the π-stacks, which produces additional space for F_4TCNQ^- to insert into the polymer crystallites.[20,21] Similar peak shifts are also observed for unaligned P3HT, as shown in SI Figures S1, S2.[58] Importantly, the data presented in Figures S1, S2, 3, and 4 indicate that this structural change is not a gradual process but instead a sharp first-order phase transition that occurs at very low doping levels. The lattice rearranges and expands to make space for the dopant counterion, in a structural change that is shown in Figure 4f. After the phase transition, only small additional structural changes generally occur as the doping level is increased over a large range. This sharp structural change allows us to define the onset of doping in each of the polymer populations. When both the doped and undoped phases are present in equal amounts, we define the system as being at the midpoint of the doping-induced phase transition. Interestingly, we find that that the face-on and edge-on polymorphs do not undergo this phase transition at the same doping concentration.

We start by examining the doping of the less-dense face-on P3HT polymorph by looking at the progression of the in-plane lamellar peaks as a function of the F_4TCNQ concentration. Figure 3b shows that the less-dense face-on polymorph possesses two lamellar (h00) peaks at a doping level of 0.02 mg/mL (inside white box), corresponding to the midpoint of the phase transition. To more accurately observe this transition, radial integrations of the lamellar peaks in Figure 3a-e are shown as 1-D patterns in Figure 4a (face-on) and Figure 4c (edge-on). The (200) peaks in Figure 4a,c are enlarged in Figure 4b,d to better see the doping-induced lamellar peak splitting. Figure 4b (orange curve) clearly shows that the less-dense face-on-oriented P3HT polymorph has a split lamellar peak when the F_4TCNQ dopant concentration is 0.02 mg/mL. At a 0.03 mg/mL F_4TCNQ concentration (Figure 4b, green curve), the phase transition is almost complete, with only a small residual undoped lamellar peak observed at ~0.76 $Å^{-1}$. The light blue and dark blue curves in Figure 4b indicate that the less-dense face-on aligned P3HT polymorph is fully doped at 0.04 mg/mL and higher F_4TCNQ concentrations.

https://doi.org/10.1021/acsmaterialslett.3c01543
ACS Materials Lett. 2024, 6, 489−497

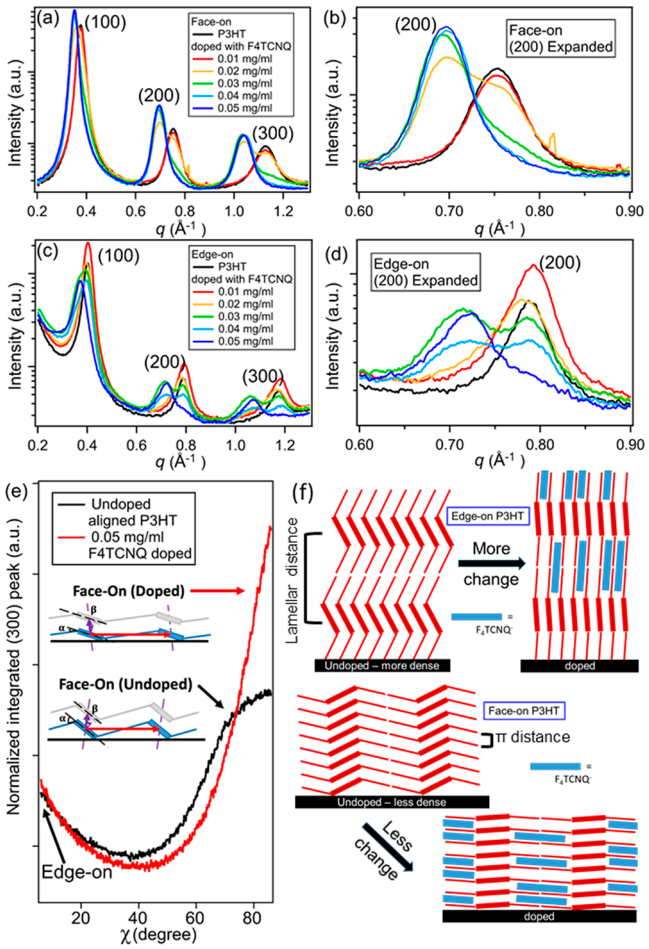

Figure 4. 1-D integrated GIWAXS patterns showing (a, c) the lamellar scattering of rub-aligned, sequentially doped P3HT films. Panel a) shows the less-dense face-on-oriented polymorph observed in the in-plane direction, and panel c) shows the denser edge-on-oriented polymorph observed in the out-of-plane direction. Panels (b,d) show zoomed-in traces of the (200) peak for both polymorphs. The double peaks indicate the coexistence of undoped and doped phases. The face-on-oriented P3HT polymorph dopes first at 0.02 mg/mL F_4TCNQ, followed by the edge-on-polymorph at 0.04 mg/mL. (e) 1-D radially integrated GIWAXS patterns of the lamellar (300) peak of undoped (black curve) and 0.05 mg/mL F_4TCNQ-doped (red curve) rub-aligned P3HT plotted against the altitudinal angle χ. Compared with undoped P3HT, the doped face-on-oriented crystallites have a narrower χ-distribution. Structural modeling indicates that the decrease in the lamellar angle during doping (inset structures, angles indicated on the χ-axis by dashed lines) is insufficient to produce the observed decrease in the χ-distribution. The change is thus attributed to the improved alignment of the doped face-on crystallites with respect to the substrate. See the SI for modeling details. (f) Cartoons of the structural changes that occur in the face-on and edge-on domains upon doping.

Next, we inspect the doping process of the denser edge-on P3HT polymorph by observing the progression of the out-of-plane (h00) peaks. Crucially, the edge-on polymorph does not show doubled (h00) peaks at a doping level of 0.02 mg/mL F_4TCNQ, a concentration for which (h00) peak splitting is observed for the face-on polymorph (Figure 3b). This indicates that the edge-on and face-on polymorphs become doped at different dopant concentrations because the two polymorphs have a different ease of doping. Instead, the edge-on aligned P3HT polymorph starts its phase transition process at a higher dopant concentration of 0.03 mg/mL F_4TCNQ (Figure 3c) and has approximately equal peak heights at 0.04 mg/mL F_4TCNQ (Figure 3d, inside the white box). The green and light blue curves in Figure 4d confirm that the doping-induced phase transition for the edge-on polymorph occurs around 0.04 mg/mL F_4TCNQ. This phase transition is then complete at 0.05 mg/mL F_4TCNQ (dark blue curve). Overall, the data clearly show that in rub-aligned P3HT films contain two different populations and that the less-dense, face-on polymorph dopes first and then, only at higher dopant concentrations, does the denser, edge-on polymorph dope.

The observed dependence of the doping order on the initial crystallite orientation leads to the question of whether the difference in doping onset for the face-on-oriented and edge-on-oriented polymorphs in aligned P3HT films is due to different doping energetics or different doping kinetics. For example, if the face-on-oriented crystallites were primarily located at the upper part of the film because of the rubbing process, it could be kinetically easier to deliver F_4TCNQ to those top domains during solution doping, compared to crystallites located closer to the substrate. This is potentially an issue because the data shown in Figures 3 and 4 were taken on rub-aligned P3HT films that were sequentially doped using acetonitrile (ACN), which does not swell the films significantly, leading to slow F_4TCNQ diffusion kinetics. Thus, to make sure that F_4TCNQ diffusion was not controlling the observed order of the doping phase transition, we repeated the experiment using dichloromethane (DCM) as the doping solvent. DCM is an excellent swelling solvent for P3HT,[59] allowing large molecules like fullerenes[17] or dodecaborane derivatives[27] to penetrate through thick polymer films all the way to the substrate. Figure 3f (along with additional data in SI Figures S3 and S4) shows that the use of DCM lowers the concentration needed to start the doping phase transition to 0.01 mg/mL F_4TCNQ for the less-dense face-on polymorph, consistent with better swelling and easier dopant infiltration. However, the data show that even with DCM as the solvent, the standard face-on-oriented P3HT polymorph still dopes first, and the denser edge-on polymorph does not dope until 0.03 mg/mL F_4TCNQ (Figure S3), producing the exact same trend as that seen with ACN. This finding indicates that any kinetic limitations of solvent swelling are not enough to explain the observed orientation-dependent doping order, leading to the conclusion that the propensity of the face-on polymorph to dope first must be a thermodynamic effect that results from the added energy penalty of rearranging the denser edge-on polymorph.

To better understand the preferential doping of the face-on crystallites, we examined GIWAXS data on doped samples over a broader range of concentrations. Lattice spacings for the lamellar and π-stacking distances for both the doped and undoped versions of face-on-oriented, edge-on-oriented, and unaligned P3HT polymorphs are given in Table S1. As discussed above, the undoped edge-on-oriented polymorph has a smaller lamellar distance than the standard face-on polymorph in the undoped state, and this difference persists after the initial doping induced phase transitions (Figure 4). After treatment with 0.05 mg/mL F_4TCNQ, the lamellar spacing in the less-dense face-on polymorph expands to 18.01 Å, while the denser edge-on polymer remains at only 17.62 Å. After full doping at higher concentrations, however, the structure change in the edge-on polymorph "catches-up", and

https://doi.org/10.1021/acsmaterialslett.3c01543
ACS Materials Lett. 2024, 6, 489−497

both polymorphs approach the unaligned structure. The lamellar spacing of the unaligned P3HT sits at 18.18 Å, while the aligned face-on and edge-on lamellar distances are only slightly smaller at 18.10 and 17.95 Å, respectively (Figure S5). This indicates that more total structural change is required to make space for F_4TCNQ^- anions in the denser edge-on P3HT lattice and that only part of that change can be driven upon initial doping. Together, these results suggest that thermodynamic energy differences in the doping process for the face-on and edge-on polymorphs are the primary reason that different F_4TCNQ concentrations are needed to induce doping.[60]

The well-aligned, highly crystalline structure of these films also allows us to explore the role of substrate interactions in controlling the energetics of doping. Figure 4e shows 1-D radially integrated patterns of the χ-angular distribution (the χ-angle is defined relative to the q_z-axis, i.e., the azimuthal angle relative to the normal of the plane of the film) for the (300) lamellar peak of undoped and fully doped (0.05 mg/mL F_4TCNQ) rub-aligned P3HT. The in-plane (300) peak of the face-on-oriented polymorph has a narrower χ-angle distribution (∼15° half-width at half-maximum, HWHM) when doped than when undoped (∼30°). In contrast, the edge-on-oriented polymorph has similar HWHM values when doped (∼14°) and undoped (∼17°). As discussed above, the broad distribution in the undoped face-on case results from the tilt of the π-stacks with respect to the unit cell, which makes it difficult for the stacks to sit flat on the Si substrate (see Figure 4a, inset); it is this same tip that makes most P3HT films adopt an edge-on orientation. The reduction in the χ-angle upon doping results in part from a change in this tilt of the π-stacks relative to the substrate (estimated to be ∼12° undoped and ∼5° doped for face-on crystallites), but this alone is insufficient to produce the observed spread of angles. We hypothesize that the remaining change results from alignment of the now reasonably flat π-stacks with the flat Si substrate. This substrate alignment may add an additional energetic term that favors doping of the face-on domains, and it should also improve vertical conduction through the film. We present a detailed model for the way the crystallite orientation of the polymorphs changes upon doping in the SI in Figures S6−S10.

In summary, we have shown that rub-aligned P3HT contains two different crystalline polymorphs. First, there are the face-on domains that are less-dense than unaligned P3HT and have a crystal structure that is slightly more similar to that of doped P3HT, and edge-on domains that are more dense and have a structure that is less similar to that of doped P3HT. Second, there are edge-on domains that are compacted by the rub-alignment process and show a denser structure with a compressed lamellar spacing that is even more different from that of doped P3HT than that of unaligned samples. The two polymorphs show well-separated diffraction peaks in GIWAXS measurements, which allowed us to investigate how differences in a crystallite's initial structure change its propensity to be doped. During doping, we found that the less-dense face-on-oriented polymorph undergoes a first-order, doping-induced phase transition more easily (at lower doping concentrations) than the denser edge-on polymorph. The face-on-oriented crystallites were also observed to better align with the substrate after doping, indicating that substrate interactions may also be energetically important. The difference in propensity to dope is attributed to differences in the starting structures, which require more or less structural change to reach the final doped configuration. Canonically, only the redox energy of the dopant and the polymer are invoked in discussing how easily a polymer can be doped, but this finding suggests that the extent of structure change upon doping can also be a significant energetic term. It also suggests that designing new polymers with crystallite structures that closely resemble their doped structures is a potential strategy for inducing the formation of more stable doped phases that can be produced at lower dopant concentrations.

Although this study examined only one polymer/dopant pair, the conclusions have implications for any polymer system where the energetics of doping controls performance. For example, the electrochemical doping that occurs in organic electrochemical transistors (OECTs) induces a nearly identical phase transition through ion injection to the one described here.[61,62] Designing polymers to facilitate this structural change could positively influence the energetics of OECTs. Having an initial structure that more closely resembles the final doped state can theoretically enhance the power efficiency of OECTs by lowering the threshold voltage (V_t) between the on and off states, impacting power consumption and noise margins.[63,64] V_t is most directly linked to the electrochemical potential,[65−67] which in turn maps onto chemical potential and the dopant concentration in our chemical doping experiments. Minimizing the reorganization energy associated with chemical doping is thus a viable route to reducing V_t in OECTs.

EXPERIMENTAL SECTION

Details of the materials, characterization, and experimental methods for film alignment, structural, and spectroscopy measurements can be found in the Supporting Information.

ASSOCIATED CONTENT

Supporting Information

The Supporting Information is available free of charge at https://pubs.acs.org/doi/10.1021/acsmaterialslett.3c01543.

Materials and experimental methods, GIWAXS data for unaligned P3HT films and for aligned P3HT films doped using DCM as a solvent, numerical fits to GIWAXS data, polarized absorption data for aligned films doped using DCM as a solvent, additional radial integrations of GIWAXS data for aligned and unaligned P3HT films and detailed modeling of those radial integrations (PDF)

AUTHOR INFORMATION

Corresponding Authors

Benjamin J. Schwartz − *Department of Chemistry and Biochemistry, University of California Los Angeles, Los Angeles, California 90095-1569, United States;* orcid.org/0000-0003-3257-9152; Email: schwartz@chem.ucla.edu

Sarah H. Tolbert − *Department of Chemistry and Biochemistry, University of California Los Angeles, Los Angeles, California 90095-1569, United States; Department of Materials Science and Engineering, University of California Los Angeles, Los Angeles, California 90095-1595, United States;* orcid.org/0000-0001-9969-1582; Email: tolbert@chem.ucla.edu

https://doi.org/10.1021/acsmaterialslett.3c01543
ACS Materials Lett. 2024, 6, 489−497

Authors

Yutong Wu − *Department of Chemistry and Biochemistry, University of California Los Angeles, Los Angeles, California 90095-1569, United States*

Quynh M. Duong − *Department of Chemistry and Biochemistry, University of California Los Angeles, Los Angeles, California 90095-1569, United States;* orcid.org/0000-0002-8032-101X

Alexander F. Simafranca − *Department of Chemistry and Biochemistry, University of California Los Angeles, Los Angeles, California 90095-1569, United States;* orcid.org/0000-0002-5274-4066

Charlene Z. Salamat − *Department of Chemistry and Biochemistry, University of California Los Angeles, Los Angeles, California 90095-1569, United States;* orcid.org/0000-0001-5581-5029

Complete contact information is available at: https://pubs.acs.org/10.1021/acsmaterialslett.3c01543

Author Contributions

Y.W. and Q.M.D. contributed equally to this work. CRediT: **Yutong Wu** data curation, formal analysis, methodology, writing-original draft; **Quynh M. Duong** conceptualization, data curation, investigation, writing-review & editing; **Alexander F Simafranca** data curation, formal analysis, investigation, writing-original draft, writing-review & editing; **Charlene Z Salamat** data curation, formal analysis, writing-review & editing; **Benjamin J. Schwartz** conceptualization, funding acquisition, project administration, resources, supervision, writing-review & editing; **Sarah H. Tolbert** conceptualization, funding acquisition, project administration, resources, supervision, writing-review & editing.

Notes

The authors declare no competing financial interest.

■ ACKNOWLEDGMENTS

This work was supported by the National Science Foundation under award DMR-2105896. Additional support was provided by NSF award CHE-2305152. GIWAXS experiments were conducted at beamline 11-3 at the Stanford Synchrotron Radiation Lightsource (SLAC National Accelerator Laboratory). Use of the Stanford Synchrotron Radiation Lightsource, SLAC National Accelerator Laboratory is supported by the U.S. Department of Energy, Office of Science, Office of Basic Energy Sciences under Contract No. DE-AC02-76SF00515.

■ REFERENCES

(1) Forrest, S. R. The Path to Ubiquitous and Low-Cost Organic Electronic Appliances on Plastic. *Nature* **2004**, *428*, 911−918.

(2) Tiwari, S.; Singh, A. K.; Joshi, L.; Chakrabarti, P.; Takashima, W.; Kaneto, K.; Prakash, R. Poly-3-Hexylthiophene Based Organic Field-Effect Transistor: Detection of Low Concentration of Ammonia. *Sens. Actuators B Chem.* **2012**, *171*−*172*, 962−968.

(3) Hou, L.; Zhang, X.; Cotella, G. F.; Carnicella, G.; Herder, M.; Schmidt, B. M.; Pätzel, M.; Hecht, S.; Cacialli, F.; Samorì, P. Optically Switchable Organic Light-Emitting Transistors. *Nat. Nanotechnol.* **2019**, *14*, 347−353.

(4) Chung, D.-Y.; Huang, J.; Bradley, D. D. C.; Campbell, A. J. High Performance, Flexible Polymer Light-Emitting Diodes (PLEDs) with Gravure Contact Printed Hole Injection and Light Emitting Layers. *Org. Electron.* **2010**, *11*, 1088−1095.

(5) Rezvani, M.; Farajollahi, F.; Nikfarjam, A.; Bakhtiarpour, P.; Saydanzad, E. Effect of Solvents, Their Mixture and Thermal Annealing on the Performance of Solution Processed Polymer Light-Emitting Diodes. *Materials* **2013**, *6*, 1994−2006.

(6) Zhang, S.; Ye, L.; Hou, J. Breaking the 10% Efficiency Barrier in Organic Photovoltaics: Morphology and Device Optimization of Well-Known PBDTTT Polymers. *Adv. Energy Mater.* **2016**, *6*, No. 1502529.

(7) Nelson, J. Polymer:Fullerene Bulk Heterojunction Solar Cells. *Mater. Today* **2011**, *14*, 462−470.

(8) Qiu, L.; Zheng, X.; Zhang, J.; Yang, Y.; Cao, W.; Dong, Y.; Xia, D.; Zhou, X.; Fan, R. Insights into the Mechanism of Solid-State Metal Organic Complexes as Controllable and Stable p-Type Dopants in Efficient Planar Perovskite Solar Cells. *ACS. Appl. Mater. Interfaces* **2020**, *12*, 546−555.

(9) Tremel, K.; Ludwigs, S. Morphology of P3HT in Thin Films in Relation to Optical and Electrical Properties. In *P3HT Revisited − From Molecular Scale to Solar Cell Devices*; Advances in Polymer Science; Ludwigs, S., Ed.; Springer: Berlin, Heidelberg, 2014; Vol. *265*, pp 39−82, DOI: 10.1007/12_2014_288.

(10) Heeger, A. J. Semiconducting Polymers: The Third Generation. *Chem. Soc. Rev.* **2010**, *39*, 2354.

(11) Oba, F.; Tatsumi, K.; Adachi, H.; Tanaka, I. N - and p-Type Dopants for Cubic Silicon Nitride. *Appl. Phys. Lett.* **2001**, *78*, 1577−1579.

(12) Yang, C.; Jin, W.; Wang, J.; Ding, Y.; Nong, S.; Shi, K.; Lu, Y.; Dai, Y.; Zhuang, F.; Lei, T.; Di, C.; Zhu, D.; Wang, J.; Pei, J. Enhancing the N-Type Conductivity and Thermoelectric Performance of Donor−Acceptor Copolymers through Donor Engineering. *Adv. Mater.* **2018**, *30*, 1802850.

(13) Yoon, S. E.; Kang, Y.; Jeon, G. G.; Jeon, D.; Lee, S. Y.; Ko, S.; Kim, T.; Seo, H.; Kim, B.; Kim, J. H. Conjugated Polymers: Exploring Wholly Doped Conjugated Polymer Films Based on Hybrid Doping: Strategic Approach for Optimizing Electrical Conductivity and Related Thermoelectric Properties (Adv. Funct. Mater. 42/2020). *Adv. Funct. Mater.* **2020**, *30*, 2070276.

(14) Griggs, S.; Marks, A.; Bristow, H.; McCulloch, I. n-Type Organic Semiconducting Polymers: Stability Limitations, Design Considerations and Applications. *J. Mater. Chem. C* **2021**, *9*, 8099−8128.

(15) Noriega, R.; Rivnay, J.; Vandewal, K.; Koch, F. P. V.; Stingelin, N.; Smith, P.; Toney, M. F.; Salleo, A. A General Relationship between Disorder, Aggregation and Charge Transport in Conjugated Polymers. *Nat. Mater.* **2013**, *12*, 1038−1044.

(16) Scholes, D. T.; Yee, P. Y.; Lindemuth, J. R.; Kang, H.; Onorato, J.; Ghosh, R.; Luscombe, C. K.; Spano, F. C.; Tolbert, S. H.; Schwartz, B. J. The Effects of Crystallinity on Charge Transport and the Structure of Sequentially Processed F_4TCNQ-Doped Conjugated Polymer Films. *Adv. Funct. Mater.* **2017**, *27*, No. 1702654.

(17) Aubry, T. J.; Axtell, J. C.; Basile, V. M.; Winchell, K. J.; Lindemuth, J. R.; Porter, T. M.; Liu, J.; Alexandrova, A. N.; Kubiak, C. P.; Tolbert, S. H.; Spokoyny, A. M.; Schwartz, B. J. Dodecaborane-Based Dopants Designed to Shield Anion Electrostatics Lead to Increased Carrier Mobility in a Doped Conjugated Polymer. *Adv. Mater.* **2019**, *31*, 1805647.

(18) Alberga, D.; Perrier, A.; Ciofini, I.; Mangiatordi, G. F.; Lattanzi, G.; Adamo, C. Morphological and Charge Transport Properties of Amorphous and Crystalline P3HT and PBTTT: Insights from Theory. *Phys. Chem. Chem. Phys.* **2015**, *17*, 18742−18750.

(19) Yamashita, Y.; Tsurumi, J.; Ohno, M.; Fujimoto, R.; Kumagai, S.; Kurosawa, T.; Okamoto, T.; Takeya, J.; Watanabe, S. Efficient Molecular Doping of Polymeric Semiconductors Driven by Anion Exchange. *Nature* **2019**, *572*, 634−638.

(20) Hamidi-Sakr, A.; Biniek, L.; Bantignies, J.-L.; Maurin, D.; Herrmann, L.; Leclerc, N.; Lévêque, P.; Vijayakumar, V.; Zimmermann, N.; Brinkmann, M. A Versatile Method to Fabricate Highly In-Plane Aligned Conducting Polymer Films with Anisotropic Charge Transport and Thermoelectric Properties: The Key Role of Alkyl Side Chain Layers on the Doping Mechanism. *Adv. Funct. Mater.* **2017**, *27*, No. 1700173.

(21) Untilova, V.; Zeng, H.; Durand, P.; Herrmann, L.; Leclerc, N.; Brinkmann, M. Intercalation and Ordering of F6TCNNQ and F4TCNQ Dopants in Regioregular Poly(3-Hexylthiophene) Crystals: Impact on Anisotropic Thermoelectric Properties of Oriented Thin Films. *Macromolecules* **2021**, *54*, 6073−6084.
(22) Untilova, V.; Biskup, T.; Biniek, L.; Vijayakumar, V.; Brinkmann, M. Control of Chain Alignment and Crystallization Helps Enhance Charge Conductivities and Thermoelectric Power Factors in Sequentially Doped P3HT:F_4TCNQ Films. *Macromolecules* **2020**, *53*, 2441−2453.
(23) Kohno, S.; Yamashita, Y.; Kasuya, N.; Mikie, T.; Osaka, I.; Takimiya, K.; Takeya, J.; Watanabe, S. Controlled Steric Selectivity in Molecular Doping towards Closest-Packed Supramolecular Conductors. *Commun. Mater.* **2020**, *1*, 79.
(24) Vijayakumar, V.; Zaborova, E.; Biniek, L.; Zeng, H.; Herrmann, L.; Carvalho, A.; Boyron, O.; Leclerc, N.; Brinkmann, M. Effect of Alkyl Side Chain Length on Doping Kinetics, Thermopower, and Charge Transport Properties in Highly Oriented F_4TCNQ-Doped PBTTT Films. *ACS Appl. Mater. Interfaces.* **2019**, *11*, 4942−4953.
(25) Karpov, Y.; Kiriy, N.; Formanek, P.; Hoffmann, C.; Beryozkina, T.; Hambsch, M.; Al-Hussein, M.; Mannsfeld, S. C. B.; Büchner, B.; Debnath, B.; Bretschneider, M.; Krupskaya, Y.; Lissel, F.; Kiriy, A. Sequentially Processed P3HT/CN6-CP $^{\bullet-}$ NBu^{4+} Films: Interfacial or Bulk Doping? *Adv. Electron. Mater.* **2020**, *6*, 1901346.
(26) Kiefer, D.; Kroon, R.; Hofmann, A. I.; Sun, H.; Liu, X.; Giovannitti, A.; Stegerer, D.; Cano, A.; Hynynen, J.; Yu, L.; Zhang, Y.; Nai, D.; Harrelson, T. F.; Sommer, M.; Moulé, A. J.; Kemerink, M.; Marder, S. R.; McCulloch, I.; Fahlman, M.; Fabiano, S.; Müller, C. Double Doping of Conjugated Polymers with Monomer Molecular Dopants. *Nat. Mater.* **2019**, *18*, 149−155.
(27) Aubry, T. J.; Winchell, K. J.; Salamat, C. Z.; Basile, V. M.; Lindemuth, J. R.; Stauber, J. M.; Axtell, J. C.; Kubena, R. M.; Phan, M. D.; Bird, M. J.; Spokoyny, A. M.; Tolbert, S. H.; Schwartz, B. J. Tunable Dopants with Intrinsic Counterion Separation Reveal the Effects of Electron Affinity on Dopant Intercalation and Free Carrier Production in Sequentially Doped Conjugated Polymer Films. *Adv. Funct. Mater.* **2020**, *30*, 2001800.
(28) Thomas, E. M.; Davidson, E. C.; Katsumata, R.; Segalman, R. A.; Chabinyc, M. L. Branched Side Chains Govern Counterion Position and Doping Mechanism in Conjugated Polythiophenes. *ACS Macro. Lett.* **2018**, *7*, 1492−1497.
(29) Jacobs, I. E.; Cendra, C.; Harrelson, T. F.; Bedolla Valdez, Z. I.; Faller, R.; Salleo, A.; Moulé, A. J. Polymorphism Controls the Degree of Charge Transfer in a Molecularly Doped Semiconducting Polymer. *Mater. Horiz.* **2018**, *5*, 655−660.
(30) Stanfield, D. A.; Wu, Y.; Tolbert, S. H.; Schwartz, B. J. Controlling the Formation of Charge Transfer Complexes in Chemically Doped Semiconducting Polymers. *Chem. Mater.* **2021**, *33*, 2343−2356.
(31) Kayunkid, N.; Uttiya, S.; Brinkmann, M. Structural Model of Regioregular Poly(3-Hexylthiophene) Obtained by Electron Diffraction Analysis. *Macromolecules* **2010**, *43*, 4961−4967.
(32) Aubry, T. J.; Ferreira, A. S.; Yee, P. Y.; Aguirre, J. C.; Hawks, S. A.; Fontana, M. T.; Schwartz, B. J.; Tolbert, S. H. Processing Methods for Obtaining a Face-On Crystalline Domain Orientation in Conjugated Polymer-Based Photovoltaics. *J. Phys. Chem. C* **2018**, *122*, 15078−15089.
(33) Guo, X.; Marks, T. J. Plastic Solar Cells with Engineered Interfaces. In *Proc. SPIE 8622, Organic Photonic Materials and Devices XV*; Tabor, C. E., Kajzar, F., Kaino, T., Koike, Y., Eds.; 2013; p 86220K, DOI: 10.1117/12.2013491.
(34) Watanabe, S.; Tanaka, H.; Ito, H.; Kuroda, S.; Mori, T.; Marumoto, K.; Shimoi, Y. Direct Determination of Interfacial Molecular Orientations in Field-Effect Devices of P3HT/PCBM Composites by Electron Spin Resonance. *Org. Electron.* **2011**, *12*, 716−723.
(35) Skrypnychuk, V.; Boulanger, N.; Yu, V.; Hilke, M.; Mannsfeld, S. C. B.; Toney, M. F.; Barbero, D. R. Enhanced Vertical Charge Transport in a Semiconducting P3HT Thin Film on Single Layer Graphene. *Adv. Funct. Mater.* **2015**, *25*, 664−670.
(36) Meredig, B.; Salleo, A.; Gee, R. Ordering of Poly(3-Hexylthiophene) Nanocrystallites on the Basis of Substrate Surface Energy. *ACS Nano* **2009**, *3*, 2881−2886.
(37) Agbolaghi, S.; Abbaspoor, S.; Massoumi, B.; Sarvari, R.; Sattari, S.; Aghapour, S.; Charoughchi, S. Conversion of Face-On Orientation to Edge-On/Flat-On in Induced-Crystallization of Poly(3-hexylthiophene) via Functionalization/Grafting of Reduced Graphene Oxide with Thiophene Adducts. *Macromol. Chem. Phys.* **2018**, *219*, 1700484.
(38) Piliego, C.; Holcombe, T. W.; Douglas, J. D.; Woo, C. H.; Beaujuge, P. M.; Fréchet, J. M. J. Synthetic Control of Structural Order in *N*-Alkylthieno[3,4-*c*]Pyrrole-4,6-Dione-Based Polymers for Efficient Solar Cells. *J. Am. Chem. Soc.* **2010**, *132*, 7595−7597.
(39) Chen, M. S.; Niskala, J. R.; Unruh, D. A.; Chu, C. K.; Lee, O. P.; Fréchet, J. M. J. Control of Polymer-Packing Orientation in Thin Films through Synthetic Tailoring of Backbone Coplanarity. *Chem. Mater.* **2013**, *25*, 4088−4096.
(40) Imanishi, M.; Kajiya, D.; Koganezawa, T.; Saitow, K. Uniaxial Orientation of P3HT Film Prepared by Soft Friction Transfer Method. *Sci. Rep.* **2017**, *7*, No. 5141.
(41) Li, J.; Xue, M.; Xue, N.; Li, H.; Zhang, L.; Ren, Z.; Yan, S.; Sun, X. Highly Anisotropic P3HT Film Fabricated via Epitaxy on an Oriented Polyethylene Film and Solvent Vapor Treatment. *Langmuir* **2019**, *35*, 7841−7847.
(42) Suzuki, S.; Sugimura, R.; Kozaki, M.; Keyaki, K.; Nozaki, K.; Ikeda, N.; Akiyama, K.; Okada, K. Highly Efficient Photoproduction of Charge-Separated States in Donor−Acceptor-Linked Bis(Acetylide) Platinum Complexes. *J. Am. Chem. Soc.* **2009**, *131*, 10374−10375.
(43) Nagamatsu, S.; Takashima, W.; Kaneto, K.; Yoshida, Y.; Tanigaki, N.; Yase, K.; Omote, K. Backbone Arrangement in "Friction-Transferred" Regioregular Poly(3-Alkylthiophene)s. *Macromolecules* **2003**, *36*, 5252−5257.
(44) Pandey, M.; Nagamatsu, S.; Pandey, S. S.; Hayase, S.; Takashima, W. Enhancement of Carrier Mobility along with Anisotropic Transport in Non-Regiocontrolled Poly (3-Hexylthiophene) Films Processed by Floating Film Transfer Method. *Org. Electron.* **2016**, *38*, 115−120.
(45) Rivnay, J.; Mannsfeld, S. C. B.; Miller, C. E.; Salleo, A.; Toney, M. F. Quantitative Determination of Organic Semiconductor Microstructure from the Molecular to Device Scale. *Chem. Rev.* **2012**, *112*, 5488−5519.
(46) Biniek, L.; Pouget, S.; Djurado, D.; Gonthier, E.; Tremel, K.; Kayunkid, N.; Zaborova, E.; Crespo-Monteiro, N.; Boyron, O.; Leclerc, N.; Ludwigs, S.; Brinkmann, M. High-Temperature Rubbing: A Versatile Method to Align π-Conjugated Polymers without Alignment Substrate. *Macromolecules* **2014**, *47*, 3871−3879.
(47) Hartmann, L.; Tremel, K.; Uttiya, S.; Crossland, E.; Ludwigs, S.; Kayunkid, N.; Vergnat, C.; Brinkmann, M. 2D Versus 3D Crystalline Order in Thin Films of Regioregular Poly(3-Hexylthiophene) Oriented by Mechanical Rubbing and Epitaxy. *Adv. Funct. Mater.* **2011**, *21*, 4047−4057.
(48) Hamidi-Sakr, A.; Biniek, L.; Fall, S.; Brinkmann, M. Precise Control of Lamellar Thickness in Highly Oriented Regioregular Poly(3-Hexylthiophene) Thin Films Prepared by High-Temperature Rubbing: Correlations with Optical Properties and Charge Transport. *Adv. Funct. Mater.* **2016**, *26*, 408−420.
(49) Ghosh, R.; Pochas, C. M.; Spano, F. C. Polaron Delocalization in Conjugated Polymer Films. *J. Phys. Chem. C* **2016**, *120*, 11394−11406.
(50) Ghosh, R.; Luscombe, C. K.; Hambsch, M.; Mannsfeld, S. C. B.; Salleo, A.; Spano, F. C. Anisotropic Polaron Delocalization in Conjugated Homopolymers and Donor−Acceptor Copolymers. *Chem. Mater.* **2019**, *31*, 7033−7045.
(51) Clark, J.; Chang, J.-F.; Spano, F. C.; Friend, R. H.; Silva, C. Determining Exciton Bandwidth and Film Microstructure in Polythiophene Films Using Linear Absorption Spectroscopy. *Appl. Phys. Lett.* **2009**, *94*, 163306.

(52) Hexemer, A.; Müller-Buschbaum, P. Advanced Grazing-Incidence Techniques for Modern Soft-Matter Materials Analysis. *IUCrJ.* **2015**, *2*, 106−125.
(53) Scholes, D. T.; Hawks, S. A.; Yee, P. Y.; Wu, H.; Lindemuth, J. R.; Tolbert, S. H.; Schwartz, B. J. Overcoming Film Quality Issues for Conjugated Polymers Doped with F_4TCNQ by Solution Sequential Processing: Hall Effect, Structural, and Optical Measurements. *J. Phys. Chem. Lett.* **2015**, *6*, 4786−4793.
(54) Bredas, J. L.; Street, G. B. Polarons, Bipolarons, and Solitons in Conducting Polymers. *Acc. Chem. Res.* **1985**, *18*, 309−315.
(55) Nagamatsu, S.; Pandey, S. S. Ordered Arrangement of F4TCNQ Anions in Three-Dimensionally Oriented P3HT Thin Films. *Sci. Rep.* **2020**, *10*, No. 20020.
(56) Stanfield, D. A.; Mehmedović, Z.; Schwartz, B. J. Vibrational Stark Effect Mapping of Polaron Delocalization in Chemically Doped Conjugated Polymers. *Chem. Mater.* **2021**, *33*, 8489−8500.
(57) Voss, M. G.; Scholes, D. T.; Challa, J. R.; Schwartz, B. J. Ultrafast Transient Absorption Spectroscopy of Doped P3HT Films: Distinguishing Free and Trapped Polarons. *Faraday Discuss.* **2019**, *216*, 339−362.
(58) Cook, J. B.; Lin, T. C.; Kim, H.-S.; Siordia, A.; Dunn, B. S.; Tolbert, S. H. Suppression of Electrochemically Driven Phase Transitions in Nanostructured MoS_2 Pseudocapacitors Probed Using *Operando* X-Ray Diffraction. *ACS Nano* **2019**, *13*, 1223.
(59) Aguirre, J. C.; Hawks, S. A.; Ferreira, A. S.; Yee, P.; Subramaniyan, S.; Jenekhe, S. A.; Tolbert, S. H.; Schwartz, B. J. Sequential Processing for Organic Photovoltaics: Design Rules for Morphology Control by Tailored Semi-Orthogonal Solvent Blends. *Adv. Energy Mater.* **2015**, *5*, No. 1402020.
(60) Wu, E. C.-K.; Salamat, C. Z.; Tolbert, S. H.; Schwartz, B. J. Molecular Dynamics Study of the Thermodynamics of Integer Charge Transfer vs Charge-Transfer Complex Formation in Doped Conjugated Polymers. *ACS Appl. Mater. Interfaces* **2022**, *14*, 26988−27001.
(61) Das, P.; Zayat, B.; Wei, Q.; Salamat, C. Z.; Magdău, I. B.; Elizalde-Segovia, R.; Rawlings, D.; Lee, D.; Pace, G.; Irshad, A.; Ye, L.; Schmitt, A.; Segalman, R. A.; Miller, T. F.; Tolbert, S. H.; Dunn, B. S.; Narayan, S. R.; Thompson, B. C. Dihexyl-Substituted Poly(3,4-Propylenedioxythiophene) as a Dual Ionic and Electronic Conductive Cathode Binder for Lithium-Ion Batteries. *Chem. Mater.* **2020**, *32*, 9176−9189.
(62) Bischak, C. G.; Flagg, L. Q.; Yan, K.; Rehman, T.; Davies, D. W.; Quezada, R. J.; Onorato, J. W.; Luscombe, C. K.; Diao, Y.; Li, C. Z.; Ginger, D. S. A Reversible Structural Phase Transition by Electrochemically-Driven Ion Injection into a Conjugated Polymer. *J. Am. Chem. Soc.* **2020**, *142*, 7434−7442.
(63) Doris, S. E.; Pierre, A.; Street, R. A. Dynamic and Tunable Threshold Voltage in Organic Electrochemical Transistors. *Adv. Mater.* **2018**, *30*, 1706757.
(64) Tan, S. T. M.; Lee, G.; Denti, I.; LeCroy, G.; Rozylowicz, K.; Marks, A.; Griggs, S.; McCulloch, I.; Giovannitti, A.; Salleo, A. Tuning Organic Electrochemical Transistor Threshold Voltage Using Chemically Doped Polymer Gates. *Adv. Mater.* **2022**, *34*, 2202359.
(65) Cendra, C.; Giovannitti, A.; Savva, A.; Venkatraman, V.; McCulloch, I.; Salleo, A.; Inal, S.; Rivnay, J. Role of the Anion on the Transport and Structure of Organic Mixed Conductors. *Adv. Funct. Mater.* **2019**, *29*, 1807034.
(66) Flagg, L. Q.; Bischak, C. G.; Onorato, J. W.; Rashid, R. B.; Luscombe, C. K.; Ginger, D. S. Polymer Crystallinity Controls Water Uptake in Glycol Side-Chain Polymer Organic Electrochemical Transistors. *J. Am. Chem. Soc.* **2019**, *141*, 4345−4354.
(67) Schmode, P.; Savva, A.; Kahl, R.; Ohayon, D.; Meichsner, F.; Dolynchuk, O.; Thurn-Albrecht, T.; Inal, S.; Thelakkat, M. The Key Role of Side Chain Linkage in Structure Formation and Mixed Conduction of Ethylene Glycol Substituted Polythiophenes. *ACS Appl. Mater. Interfaces* **2020**, *12*, 13029−13039.

https://doi.org/10.1021/acsmaterialslett.3c01543
ACS Materials Lett. 2024, 6, 489−497